Indian J Phys (September 2021) 95(9):1853–1863
https://doi.org/10.1007/s12648-020-01848-7

ORIGINAL PAPER

Optical constants and dispersion parameters of amorphous $Se_{65-x}As_{35}Sb_x$ thick films for optoelectronics

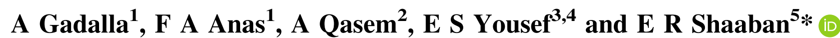
A Gadalla[1], F A Anas[1], A Qasem[2], E S Yousef[3,4] and E R Shaaban[5]*

[1]Physics Department, Faculty of Science, Assiut University, Assiut, Egypt

[2]Physics Department, Faculty of Science, Al-Azhar University, Nasr City, Cairo 11884, Egypt

[3]Physics Department, Faculty of Science, King Khalid University, P.O. Box 9004, Abha, Saudi Arabia

[4]Research Center for Advanced Materials Science (RCAMS), King Khalid University, P.O. Box 9004, Abha 61413, Saudi Arabia

[5]Physics Department, Faculty of Science, A1-Azhar University, Assiut 71542, Egypt

Received: 18 October 2019 / Accepted: 03 April 2020 / Published online: 8 October 2020

Abstract: Optical properties of amorphous $Se_{65-x}As_{35}Sb_x$ thin films with different compositions (x = 0, 2, 4, 6, 8 and 10 at%) deposited by evaporation technique have been investigated by measuring transmission (T) and reflection (R) in the wavelength range 400–2500 nm. An optical characterization method for uniform films based on Swanepoel's method has been employed to extract the refractive index n and film thickness d, with high precision (better than 1%). The calculated thickness for all thin films was about 1 µm. In addition, the absorption coefficient was evaluated in the strong absorption region of T and R. The possible optical transition in these films is found to be allowed indirect transition with energy gap E_g^{opt} decreases from 1.72 to 1.53 eV with increasing Sb content at expense of Se. The chemical bond approach has been applied to explain the decrease of the optical gap with increasing Sb content. The dispersion and oscillator energies were analyzed using the concept of the single oscillator by Wemple and Di-Domenico. The nonlinear refractive index was calculated and found to be increase with increasing Sb content.

Keywords: $Se_{65-x}As_{35}Sb_x$; Optical constants; Linear and nonlinear refractive index; Loss functions

1. Introduction

Chalcogenide glasses contain one or more chalcogen element (Se, S, Te) which produces covalent bonds with the network formers like As, Sb, Ge, etc. Because of the high atomic masses and hence the low phonon energies in these elements, the transmission range extends into infrared region making it a suitable candidate for many applications in medical imaging, telecommunication, bio-sensing, infrared waveguides, optical fibers [1–4]. These materials appear a continuous alteration in many physical properties with alteration in chemical composition [5]. Many investigations of the electrical properties [6, 7], photo-conductivity [8], glass formation [9], study of structure [10] and analysis of crystallization kinetics [11–13] of the glassy (As–Se–Sb) system have been made. To our knowledge, less detailed investigations have been performed on their optical properties. In addition, more efforts have been carried out to develop the mathematical formulation describing both the reflectance and the transmittance of different optical systems. In the present work, the optical properties of amorphous semiconductor $Se_{65-x}As_{35}Sb_x$ (0 $\le \leftarrow x \leftarrow \le \leftarrow$10) thin films are investigated. The straightforward method proposed by Swanepoel is applied which is based on the use of the extremes of the interference fringes of transmittance spectrum for calculation the refractive index and film thickness in the transparent region. For determination of the refractive index, the film thickness of the samples must be sufficient high (about 1 µm) in order to obtain several interference extremes and help us to avoid the effect of the film thickness on the optical constants of the films. The absorption coefficient therefore band gap is calculated in the strong absorption region of transmittance and reflectance spectra. The dispersion parameters are

*Corresponding author, E-mail: esam_ramadan2008@yahoo.com

© 2020 IACS

discussed using by Single-oscillator Wemple-Di Domenico model [14]. The compositional variation of optical band gap with Se-As-Sb thin films is discussed in terms of the chemical bond approaches present in the glassy compositions under study.

2. Experimental procedures

Bulk chalcogenide $Se_{65-x}As_{35}Sb_x$ with ($0 \leq x \geq 10$) at. % was prepared by the usual melt quench technique. Highly pure materials (99.999%) were weighted based on their atomic percentages, using an electrical balance type (Sartorius) with accuracy ($\pm 10^{-4}$ g) and sealed in evacuated silica tube (10^{-3} Pa) and it was heated at 1000 °C with the temperature ramp about 5 °C/min for 24 h. During the melting process, the ampoule was inverted at regular time intervals ($\sim$ 1 h) so that the amorphous solid will be homogenous and isotropic. After the synthesis, the melt was quenched rapidly in ice water to obtain the $Se_{65-x}As_{35}Sb_x$ glassy alloy. Then the solid was broken along its natural stress line into smaller pieces suitable for grinding. The different compositions of $Se_{65-x}As_{35}Sb_x$ with ($0 \leq x \geq 10$ at%) thin films were deposited by evaporating the powdered chalcogenide samples from a resistance heating quartz glass crucible onto dried precleaned glass substrates kept at room temperature, using a conventional coating unit (Denton Vacuum DV 502 A). The films were deposited onto glass substrates at a pressure of about 1×10^{-6} Pa. Both the film thickness and the deposition rate (was about 20 Å/s) were monitored using FTM6 thickness monitor. The elemental composition of the films was analyzed using energy-dispersive X-ray spectrometer (EDX) interfaced with a scanning electron microscope, SEM (JOEL XL) operating an accelerating voltage of 30 kV. The relative error of determining the indicated elements does not exceed 2%. X-ray powder diffraction (XRD) Philips diffractometry (1710), with Cu-Kα1 radiation (λ = 1.54056 Å) has been used to examine the structure of the as-prepared thin films. The data collection was performed by step scan mode, in a 2θ range between 5° and 90° with step-size of 0.02° and step time of 0.6 s. The transmittance (T) and reflectance (R) optical spectra of the as-deposited films were performed at room temperature range using UV-Vis-NIR SHIMADZU UV-1700 double beam spectrophotometer. At normal incidence, the transmittance spectra were collected without substrate in the reference beam in the wavelength range 400–2500 nm, while the reflectance spectra were measured using reflection attachment close to normal incidence ($\sim$ 5°).

3. Results and discussion

3.1. XRD analysis

Figure 1 demonstrates XRD patterns of different compositions of $Se_{65-x}As_{35}Sb_x$ with ($0 \leq x \geq 10$ at. %.) Such a figure revealed broad peaks without any sharp crystallization peaks, suggesting that the amorphous nature of such films.

3.2. Optical studies

3.2.1. Interference fringes in transmittance spectra

The optical properties were studied for as-prepared $Se_{65-x}As_{35}Sb_x$ by optical transmittance [T (λ)] and the reflectance [R (λ)] data of wavelength range of (400–2500 nm). The spectra of T (λ) and R (λ) for $Se_{65-x}As_{35}Sb_x$ thin films are shown in Fig. 2. The thickness of the studied samples was deduced according to Swanepoel's method, which is based on the idea of Manifacier et al. [15] of creating upper and lower envelopes of the transmittance spectrum which showed the construction of the two envelopes T_M (λ), T_m (λ) (according to Eq. (1)) and then the geometric mean:

$$T_\alpha = \sqrt{T_M(\lambda)T_m(\lambda)} \quad (1)$$

3.2.2. Envelope construction

The two envelopes construction T_M (λ) and T_m (λ) are expressing using by program origin version 2018 (OriginLab Corp.), where T_M and T_m are the transmission maximum and the corresponding minimum at a certain wavelength. Alternatively, one of these values is an empirical interference extreme and the other one is derived from the corresponding envelope; both envelopes were computer-generated using by the program origin version 2018 (Origin-Lab Corp.). T_M (λ) and T_m (λ) are displayed in Fig. 3 and their values are listed in Tables 1.

3.2.3. Estimation of the refractive index of the substrate

The refractive index of the film substrate was determined using the subsequent relation [16]:

$$S_j = (T_{sj})^{-1} + \sqrt{((T_{sj})^{-1} + 1)} \quad (2)$$

where T_s is the transmittance of the glass substrate which has been defined by the subsequent function:

$$T_{s(j)} = A + B\lambda_j + C\lambda_j^2 + D\lambda_j^3 \quad (3)$$

where j is a number refers to a specific wavelength and the values of the constants that appear in Eq. (3), namely A, B,

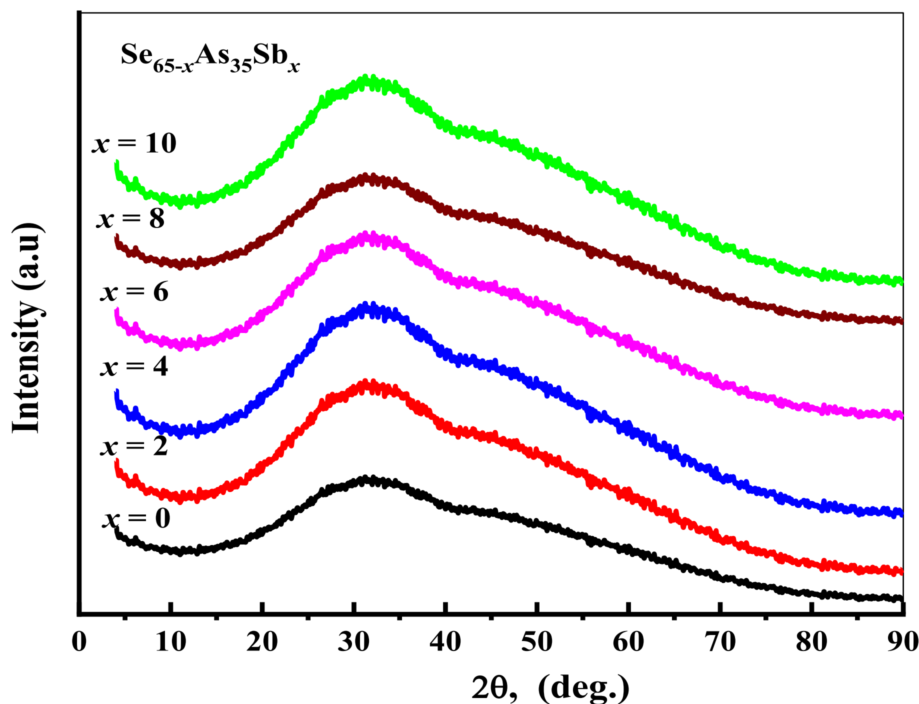

Fig. 1 The XRD patterns of different composition of $Se_{65-x}As_{35}Sb_x$ thin films onto glass substrates

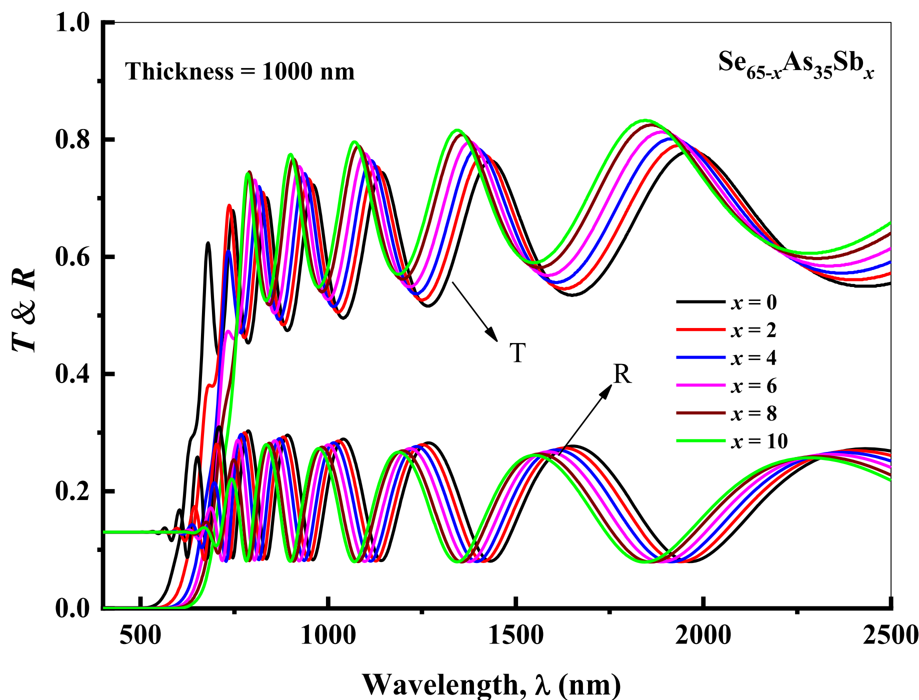

Fig. 2 Transmission and reflection spectra of $Se_{65-x}As_{35}Sb_x$ with thin films

C and D equal to 0.901414, 8.02369×10^{-5}, 6.13838×10^{-8} and 1.38877×10^{-11}, respectively.

3.2.4. Estimation of crude refractive index

The crude refractive index (n_e) of the as-prepared films under investigation can be deduced based on the envelope method via transmission spectrum proposed by Swanepoel's [17, 18]. The values of n_e can be computed at any wavelength via the following Eq. [19]:

$$n_e = [N + (N^2 - s_j^2)^{1/2}]^{1/2} \tag{4}$$

where

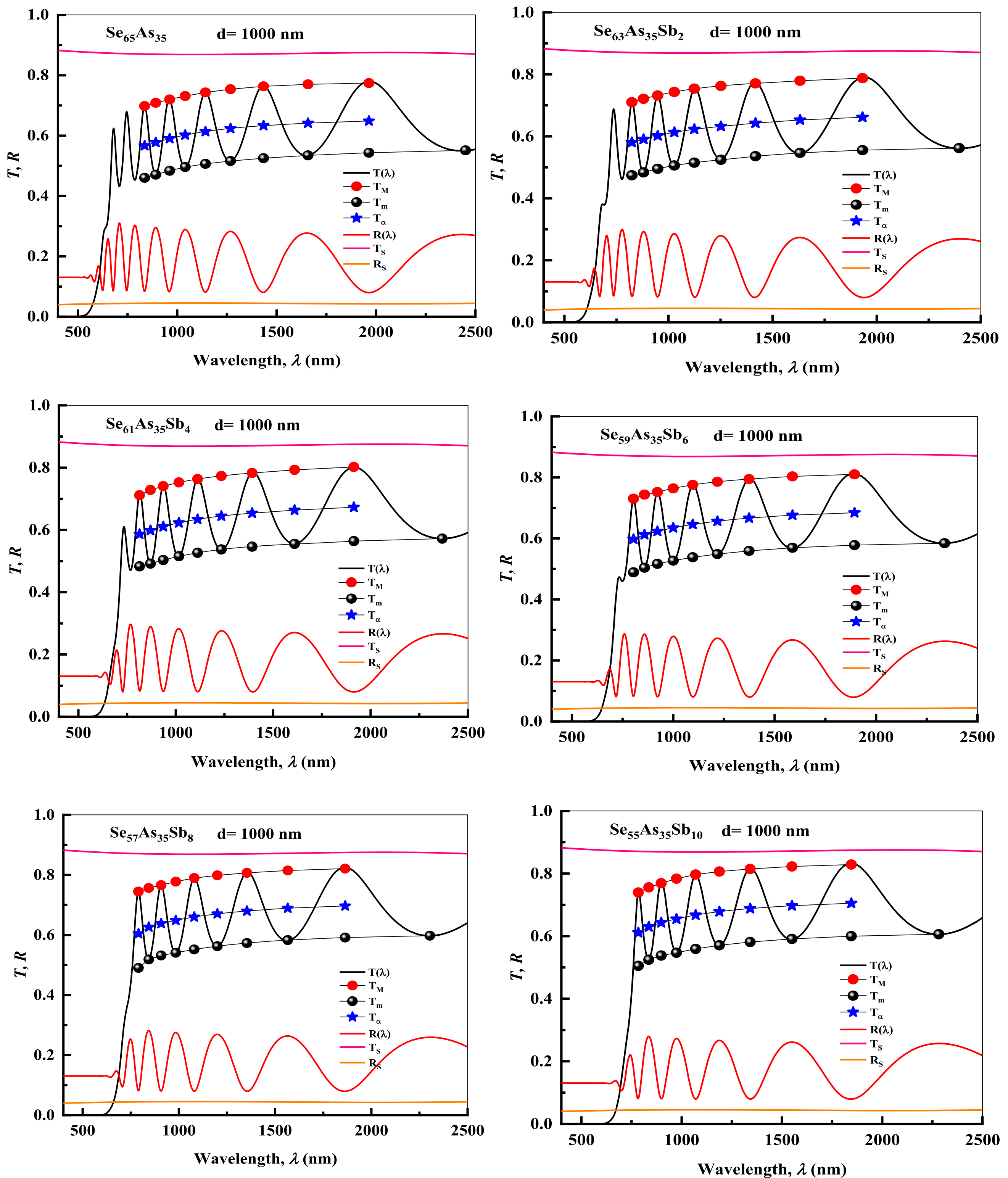

Fig. 3 Variation of the typical spectral transmittances and reflectance versus wavelength for different ratios $Se_{65-x}As_{35}Sb_x$ thin films

$$N = 2s_j \frac{T_{M_j} - T_{m_j}}{T_{M_j} T_{m_j}} + \frac{S_j^2 + 1}{2} \quad (5)$$

where s_j is *the* refractive index of the glass substrate. Values of crude refractive index, ($n_e \equiv n_1$) for two as-

Table 1 Values of the wavelength of the incident photon, the two envelopes T_M and T_m for $Se_{65-x}As_{35}Sb_x$ with ((0 ≤ x ≥ 2 at. %) thin films. The calculated values of refractive index and film thickness are based on the envelope method

X at.%	λe nm	TM	Tm	S	N1	D1 (nm)	Mo	M	D2(nm)	N2
0	836	0.6980	0.4601	1.4324	2.64	–	6.49	6.5	1026.69	2.66
	892	0.7088	0.4705	1.4333	2.61	1017.61	6.02	6	1022.32	2.62
	962	0.7200	0.4837	1.4338	2.57	1051.64	5.49	5.5	1026.81	2.58
	1040	0.7312	0.496	1.4336	2.54	1047.44	5.01	5	1023.27	2.54
	1142	0.7430	0.5065	1.4323	2.51	1033.99	4.52	4.5	1021.46	2.51
	1268	0.7539	0.5159	1.4294	2.49	1002.08	4.03	4	1017.40	2.48
	1434	0.7634	0.5253	1.4243	2.46	1003.29	3.52	3.5	1017.93	2.45
	1658	0.7700	0.5344	1.4172	2.43	–	3.00	3	1022.61	2.42
	1964	0.7741	0.5432	1.4121	2.39	–	2.50	2.5	1023.91	2.40
$\overline{d_1} = 1026.01$ nm $\sigma_1 = 19.743(1.92\%)$ $\overline{d_2} = 1022.49$ nm$\sigma_2 = 3.105(0.304\%)$										
2	824	0.71	0.4743	1.43215	2.59	–	6.49	6.5	1030.22	2.63
	880	0.7209	0.4836	1.43321	2.57	1044.09	6.03	6	1023.95	2.59
	948	0.7317	0.4951	1.43383	2.54	1081.43	5.53	5.5	1023.75	2.55
	1028	0.7431	0.506	1.43374	2.51	1051.95	5.04	5	1020.02	2.51
	1124	0.7537	0.515	1.43263	2.49	987.10	4.58	4.5	1011.768	2.48
	1252	0.7625	0.5243	1.42984	2.47	989.29	4.06	4	1012.34	2.45
	1418	0.7707	0.5358	1.42485	2.43	1024.67	3.53	3.5	1019.03	2.42
	1632	0.7794	0.5468	1.41796	2.39	–	3.02	3	1020.26	2.39
	1932	0.7878	0.5554	1.41219	2.37	–	2.53	2.5	1016.80	2.37
$\overline{d_1} = 1029.79$ nm $\sigma_1 = 33.79(3.28\%)$ $\overline{d_2} = 1019.79$ nm$\sigma_2 = 5.493(0.539\%)$										

prepared thin films with (x = 0, x = 2), as only examples, are computed and listed in Tables 1.

3.2.5. *Determination of the crude and accuracy films thickness*

Values of n_e at any adjacent maximal (or minimal), that have been computed by Eq. (4) are used to calculate crude film thickness (d_1). If n_{e1} and n_{e2} are the refractive indices of two adjacent maxima or minima at wavelengths λ_{e1} and λ_{e2}, then the crude thickness of the film is expressed as [20]:

$$d_1 = \frac{\lambda_{e1}\lambda_{e2}}{2}\left[\lambda_{e1}n_{e2} - \lambda_{e2}n_{e1}\right]^{-1} \tag{6}$$

To improve the accuracy of film thickness, there was a set of the order number (m_o) for the interference fringes was computed using by relation [20]:

$$m_0 = \frac{2n_{e1}\bar{d}_1}{\lambda_{e1}} \tag{7}$$

where ($n_e \equiv n_1$)and λ_{e1} are the values taken at the extreme point of the interference fringes and d_1 is the average of d_1 from Eq. (6) then by taking the approximate value of m_o produces a new order number m where m = 1, 2, 3… at the maximum points in the transmission spectrum and m = 1/2, 3/2, 5/2… at minimum points in the transmission spectrum after that the accuracy of refractive index (n_2) in terms of accuracy of thickness thin film expresses, (d_2) as the subsequent relation:

$$n_2 = \frac{m \cdot \lambda_{e1}}{2 \cdot \bar{d}_2} \tag{8}$$

where $\bar{d}_2$ is the new average accuracy thickness of thin films after rounded m_o to m. The final values of new refractive index n_2 and other mentioned values are presented in Table 1. On the other hand, to compute the standard deviation values (σ_i) and deviation ratio (p_i) about the actual value for each of d_1 and d_2, we used the subsequent equations:

$$\sigma_i = \left\{\left[\frac{\sum_1^n (d_i)^2}{n}\right] - (\bar{d}_1)^2\right\}^{0.5}, \quad \bar{d}_1 = \frac{\sum_1^n (d_i)}{n}, \quad P_i\% = \frac{\sigma_i}{\bar{d}_i} \times 100 \tag{9}$$

where i is a number equals to 1 or 2, and n refers to the number of thicknesses.

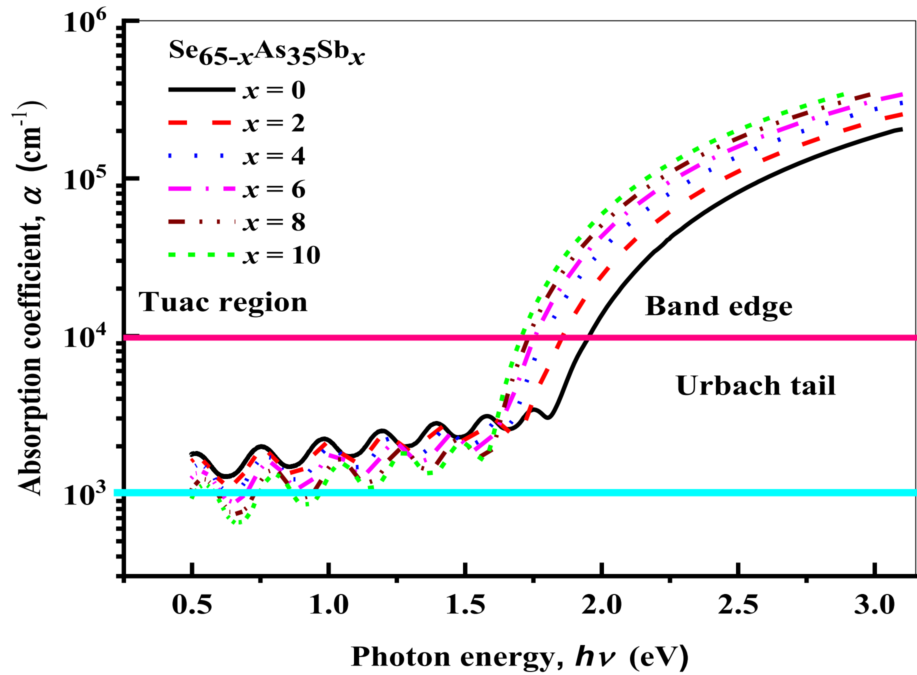

Fig. 4 The dependence of the absorption coefficient on the incident photon energy for $Se_{65-x}As_{35}Sb_x$ thin films

3.2.6. Estimation of optical parameters

The absorption coefficient (α) can be deduced in the strong absorption region via both the empirical transmission (*T*) and reflection (*R*) spectra [21–23] as follows:

$$\alpha = \frac{1}{d}\ln\left[\frac{(1-R)^2 + \sqrt{(1-R)^4 + 4(TR)^2}}{2T}\right] \quad (10)$$

where *d* is the thickness of the films that computed by Swanepoel's method and almost equals to 1 µm. Figure 4 shows the dependence of the absorption coefficient, α, on photon energy *(hv)* for amorphous $Se_{65-x}As_{35}Sb_x$ thin film with different composition, *x* = 0, 2, 4, 6, 8 and 10 at%).

It is clear that the absorption edge ($\alpha \geq 10^4$) shifts toward the lower photon energy with increasing Sb content that is related to the decreasing of the optical bandgap. Based on the Tauc's equation at the end of absorption edge region ($\alpha \geq 10^4$ cm^{-1}), the optical energy band gap (E_g) can be determined via the values of the absorption coefficient using the following Equation [24–26]:

$$\alpha(hv) = A\left(hv - E_g^{\mathrm{opt}}\right)^r \quad (11)$$

where *A* is a constant parameter and depends on the transition probability and (*r* = 2) for non-direct transition and (*r* = 1/2) for the direct transition. For investigated thin films we notice that the indirect transitions are valid. Figure 5 appears the $(\alpha hv)^{1/2}$ against *hv* for investigated samples. E_g of the films was estimated from the intercept of the linear portion of each curve for the studied films with *hv* in the abscissa, *i.e.,* at $(\alpha hv)^{1/2} = 0$ as presented in Fig. 5.

On the other hand, the absorption coefficient at less than about $\alpha \sim 10^4$ cm^{-1} near the absorption edge depends exponentially on *hv* as follows [26, 27]:

$$\alpha(hv) = \alpha_0 \cdot \exp\left[\frac{hv}{E_e}\right] \quad (12)$$

where α_o is a constant and E_e is the Urbach energy. (E_e) is computed from plotting ln(α) versus *hv* as illustrated in Fig. 6. The computed values of E_g and E_e are presented in Table 2. Apparently, the optical band gap E_g^{opt} decreases from 1.72 to 1.53 eV with increasing Sb content at expense of Se content.

3.3. Determination of the absorption constants

3.3.1. Estimation of the refractive index

Figure 7 shows the dependence of refractive index on wavelength for as-prepared thin films under investigation. In the strong absorption spectral region, the values of the refractive index can be fitted using the two-term Cauchy dispersion relationship, $n(\lambda) = a + (b/\lambda^2)$ which can be used to extrapolate the complete overall wavelengths [27]. It is clear that the refractive index increases with increasing Sb content as shown in Fig. 7. The values of Cauchy coefficients (*a* and *b)* are listed in Table 2. The increasing in refractive index is related to the increased polarizability of the larger Sb atoms (atomic radius, 1.53 Å), in comparison with Se atoms (atomic radius, 1.22 Å). One can see that the refractive index increases while optical band gap

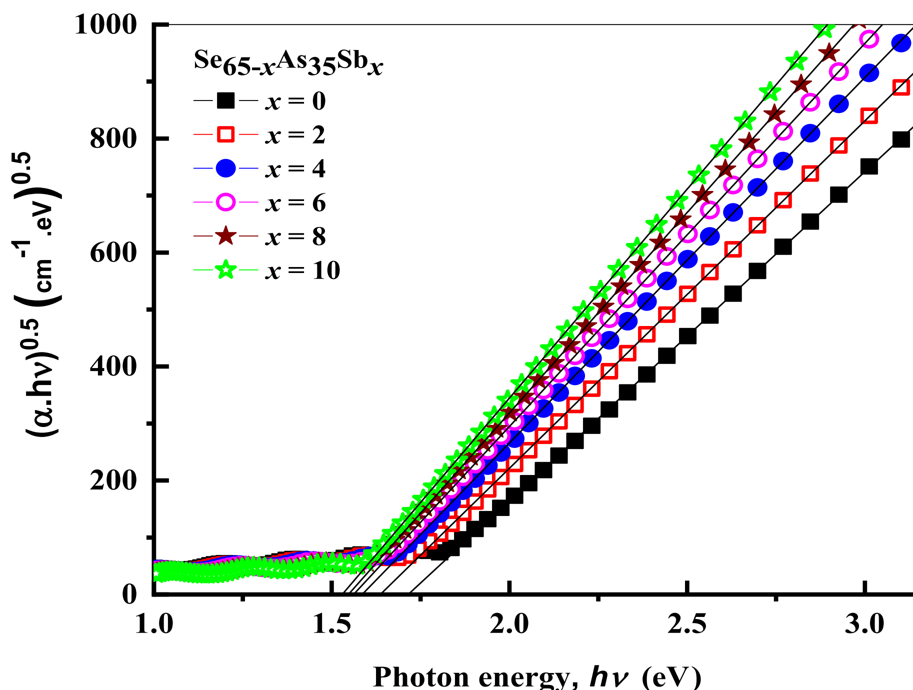

Fig. 5 The plot of $(\alpha h\nu)^{0.5}$ versus photon energy ($h\nu$) for $Se_{65-x}As_{35}Sb_x$ thin films

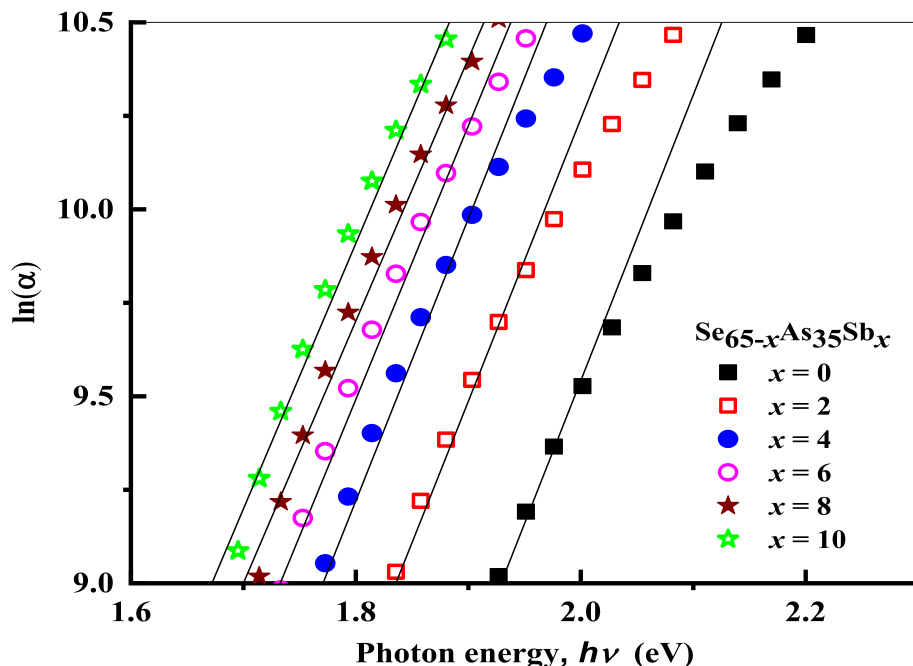

Fig. 6 The plot of $ln(\alpha)$ versus photon energy ($h\nu$) for $Se_{65-x}As_{35}Sb_x$ thin films

decreases, this behavior may be explained using Moss rule, which says n and E_g^{opt} are in inverse relation.

The variation of energy gap (E_g^{opt}) with composition in amorphous ternary alloys can be described by the following simple relation [5]:

$$E_g(AsSeSb) = aEgAs + bEgSe + cEgSb \quad (13)$$

where a, b and c are the fractions of the element As, Se and Sb, respectively. EgAs, EgSe and EgSb are the corresponding optical gaps, which equal 1.15, 1.95 and 0.15, respectively. One can see that the Sb has an energy gap lower than Se, so the calculations of E_g based on the above equation for the present $Se_{65-x}As_{35}Sb_x$ alloys cause reduction in energy gap.

The absorption index, namely the extinction coefficient ($k_{ex.}$) has been computed using the following relation [28, 29]:

Table 2 Physical parameters of the $Se_{65-x}As_{35}Sb_x$ with ((0 ≤ x ≥ 10 at. %) thin films

Comp.	Optical parameters		Dispersion parameters			Cauchy's constants	
	$E_g^{ind}(eV)$	$E_e(eV)$	$E_O(eV)$	$E_d(eV)$	$n(o)$	a	$b(\mathrm{nm})^2$
x = 0	1.719	0.131	3.645	18.34	2.46	2.34	221281.96
x = 2	1.637	0.132	3.331	18.27	2.55	2.31	218903.76
x = 4	1.589	0.133	3.189	17.89	2.57	2.29	201151.01
x = 6	1.562	0.136	3.142	17.84	2.58	2.28	192771.32
x = 8	1.549	0.140	3.095	17.73	2.59	2.25	177887.22
x = 10	1.532	0.143	3.067	17.66	2.60	2.23	176630.95

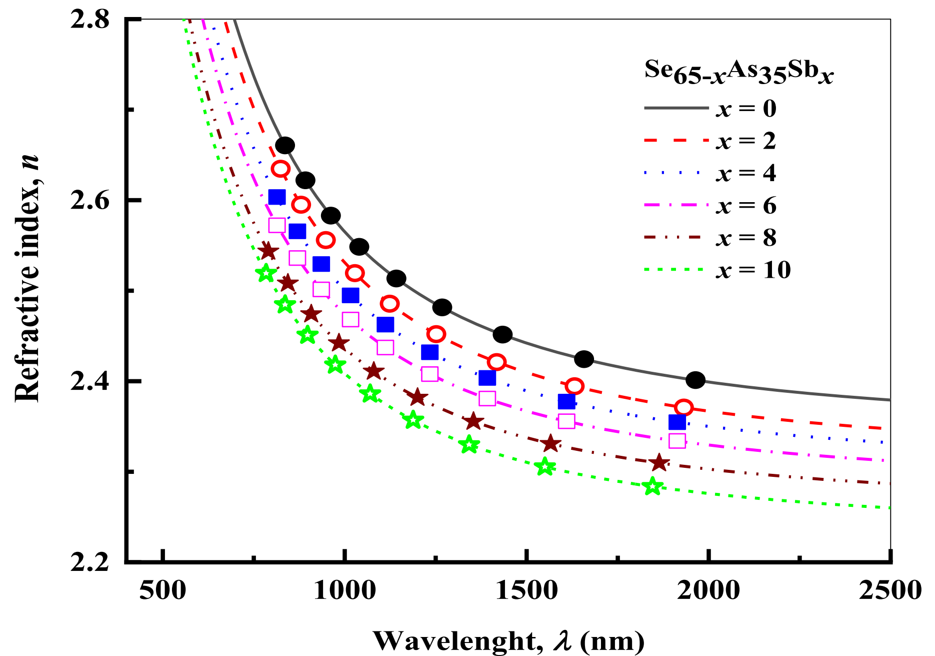

Fig. 7 The spectral dependence of refractive index (n) for $Se_{65-x}As_{35}Sb_x$ thin films

$$k_{ex.} = \varepsilon_0\,\alpha\lambda = \frac{\alpha\lambda}{4\pi} \quad (13)$$

The values of k_{ex} of investigated samples decrease with increasing the wavelength, whereas these values increase with increasing Sb content as shown in Fig. 8.

3.3.2. Determination of the loss factor

There is quantity frequently used to characterize the optical properties of thin films is called the dissipation factor (tan(δ)) which can be evaluated using the following relation [30]:

$$\tan(\delta) = \frac{\varepsilon_i}{\varepsilon_r} \quad (14)$$

Here, ε_r and ε_i represent the real ($\varepsilon_r = n^2 - k^2$) and imaginary ($\varepsilon_i = 2nk$) parts of the dielectric constant, respectively. The variations of dissipation factor as a function of photon energy were shown in Fig. 9. This figure appears that the dissipation factor increases with increasing photon energy.

3.4. Determination of the dispersion parameters

The dispersion of refractive index (n (λ)) was analyzed using by the concept of the single oscillator and can be expressed by the Wemple-Didomenico relationship [14, 31] as:

$$n^2 = 1 + \frac{E_o E_d}{E_o^2 - (hv)^2} \quad (15)$$

where (hv) is the photon energy, E_o is the oscillator energy and E_d is the dispersion energy which measures the average strength of inter-band optical transitions. Figure 10 shows

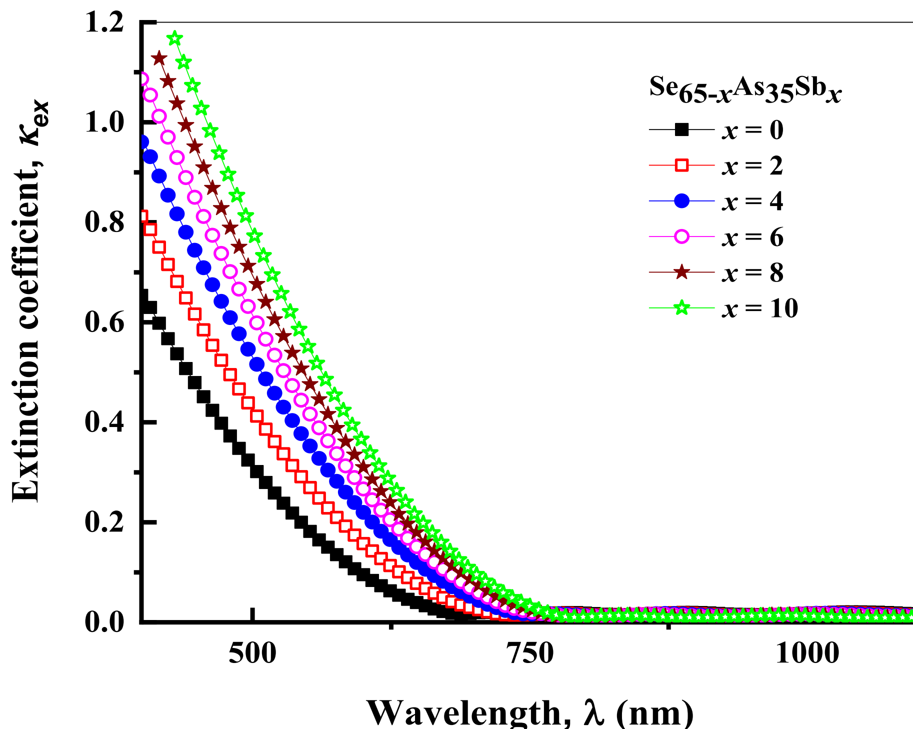

Fig. 8 Variation of extinction coefficient *(k)* versus wavelength (λ) for $Se_{65-x}As_{35}Sb_x$ with thin films

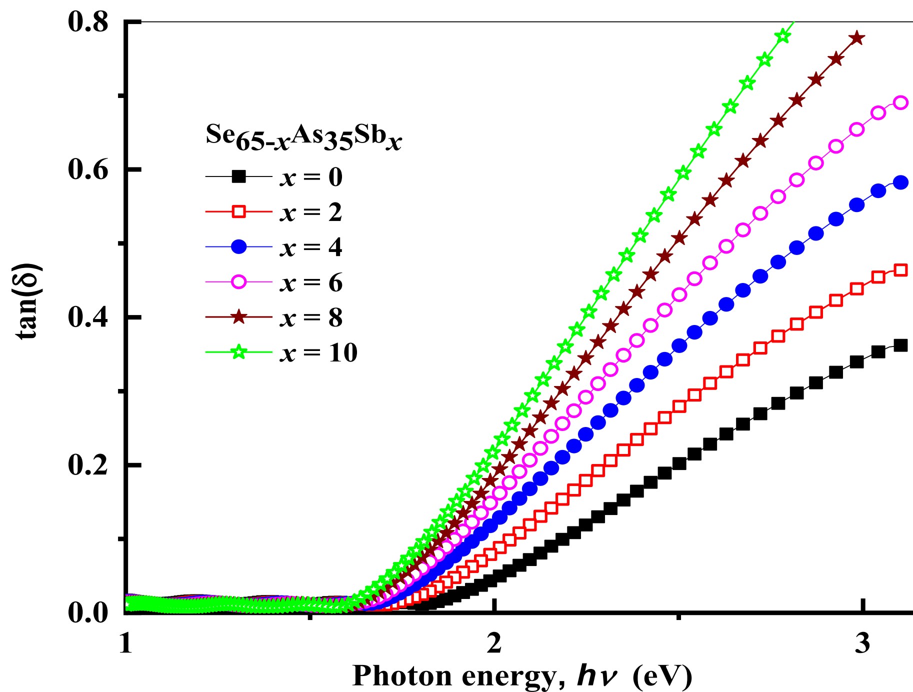

Fig. 9 Variation of dissipation factor (*tan(δ)*) on the photon energy *(hv)* for $Se_{65-x}As_{35}Sb_x$ thin films

the relation between $(n^2 - 1)^{-1}$ versus $(h\nu)^2$ for the investigated films. The values of E_d and E_o have been deduced from the slopes and the intersection of the straight lines with $(n^2 - 1)^{-1}$ axis. The variations of E_o and E_d with Sb concentration of the studied samples are illustrated in Table 2. The values of E_d and E_o decrease with increasing the Sb content. The decrease in E_o and E_d could be attributed to the increase in the number of scattering center that due to the dissolving of Sb atoms in the glass film matrix [32]. Further analysis of the $(n^2 - 1)^{-1}$ against $(h\nu)^2$ allows to deduce the static refractive index, using the subsequent relation:

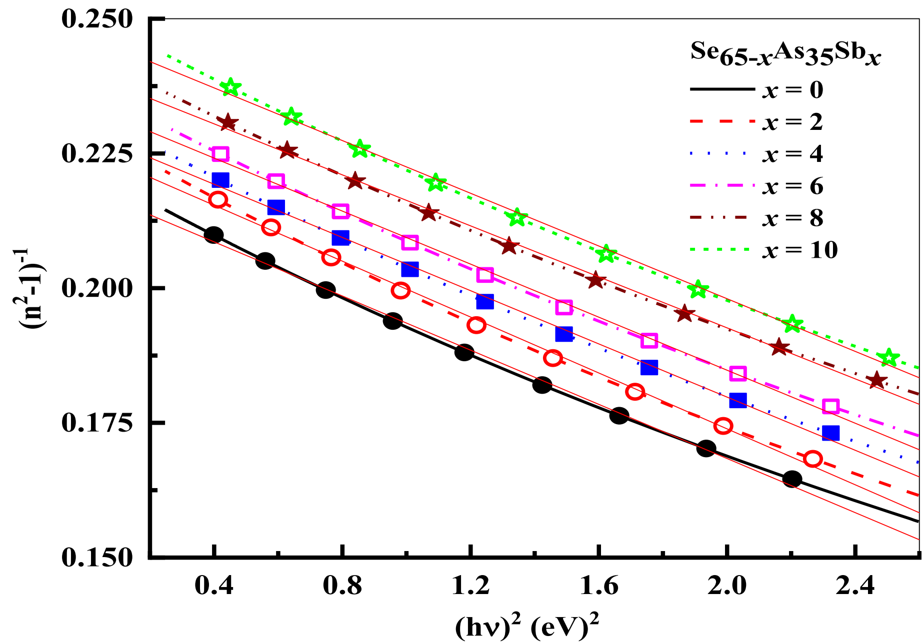

Fig. 10 The plot of the relation between $(n^2-1)^{-1}$ and $(h\nu)^2$ for the investigated compositions

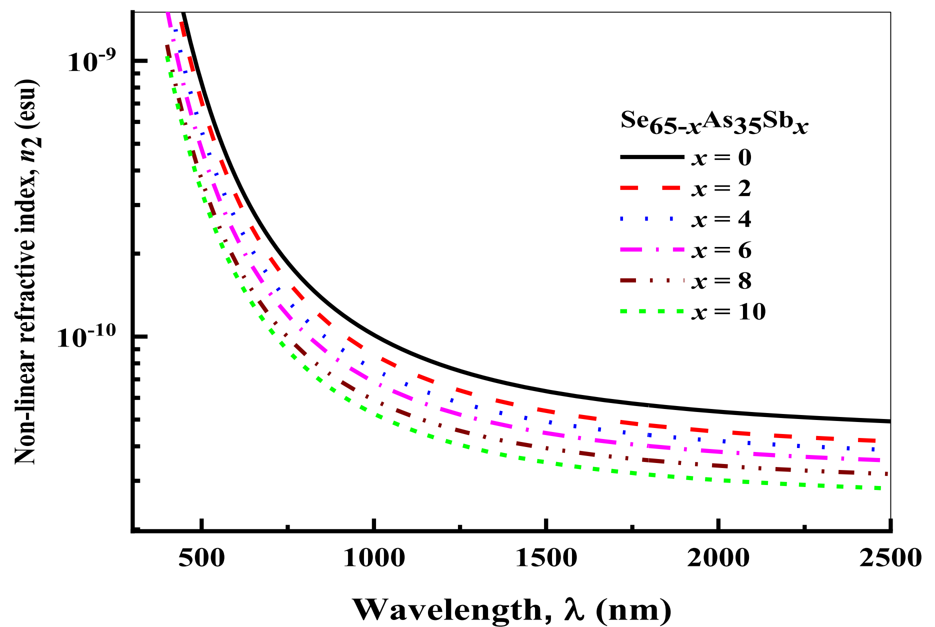

Fig. 11 Dependence of nonlinear the refractive index (n_2) on the wavelength for investigated films

$$n_o = (1 + E_d/E_0)^{1/2} \tag{16}$$

The computed values are tabulated in Table 2.

3.5. Determination of nonlinear refractive index

The strong electric field of high intensity light may cause a medium's refractive index to vary as the light passes through it, giving rise to nonlinearity. The nonlinear refractive index highly relies on incident intensity. When matter is exposed to intense electric field of incident light, polarization is no longer proportional to electric field and the change in polarizability has to be extended by terms proportional to square of electric field [33].

The nonlinear refractive index was deduced in terms of Tichy and Ticha relationship [34]. Tichy and Ticha relationship is a combination of Miller's popularized rule and static refractive index obtained from WDD model as [34]:

$$n_2 = \left[\frac{12\pi}{n_0}\right]\chi^{(3)} \tag{17}$$

where $\chi^{(3)}$ is third-order nonlinear susceptibility. $\chi^{(3)}$ is obtained from the equation [35, 36];

$$\chi^{(3)} = B[\chi^{(1)}]^4 \tag{18}$$

where $\chi^{(1)}$ is linear susceptibility and is given as:

$$\chi^{(1)} = \frac{1}{4\pi}\left[\frac{E_d}{E_o}\right] \tag{19}$$

where $B = 1.7\times10^{-10}$ (for $\chi^{(3)}$ in esu), $\chi^{(3)}$ is given as:

$$\chi^{(3)} = \frac{B}{(4\pi)^4}\left(n_o^2 - 1\right)^4 \tag{20}$$

Figure 11 shows plots of nonlinear refractive index, n_2 versus wavelength, λ. From this figure, it is found that the value of nonlinear refractive index decreases with increasing Sb content.

4. Conclusions

In summary, bulk samples of $Se_{65-x}As_{35}Sb_x$ thin films with ((0 ≤ x ≥ 10) at. %) were successfully synthesized using a homogeneous precipitation method. The studied films were deposited using thermal evaporation technique. The optical characterization of different compositions of amorphous $Se_{65-x}As_{35}Sb_x$ films has been carried out using the transmittance and reflectance spectra. The envelope method suggested by Swanepoel has been applied to the films with larger thickness, which has a reasonable number of interference fringes. The results indicate that n gradually increases with increasing Sb content. The increase in the refractive index is explained in terms of the polarizability. The dispersion of the refractive index studied utilizing the WDD single-oscillator model. The oscillator and dispersion parameters were computed. The nonlinear refractive index of the studied films is well related to the linear refractive index. Low optical transmittance and small bandgap for $Se_{65-x}As_{35}Sb_x$ films render them hopeful candidate for optoelectronic devices and so for various light detection, modulation and manipulation functions.

Acknowledgment The authors thank the Deanship of Scientific Research at King Khalid University (KKU) for funding this research project, Number: (R.G.P2./62/40) under research center for advanced material science. Both Assiut University and Al-Azhar University have also acknowledged.

References

[1] P Toupin, L Brilland, J Trolès, J L Adam *Opt. Mater. Exp.* **2** 1359 (2012)
[2] D C Sati, A Dahshanc, P Sharma *Appl. Mater. Today* **17** 142–158 (2019)
[3] WH Kim, VQ Nguyen, LB Shaw, LE Busse, C Florea, DJ Gibson, et al. *J. Non Cryst Solids* **431** 8–15 (2016)
[4] V Sharma, S Sharda, N Sharma, S C Katyalc, P Sharma *Prog. Solid State Chem.* **54** 31–44 (2019)
[5] S Fayek, A Maged, M Balboul *Vacuum* **53** 447 (1999)
[6] E R Shaaban, I Kansal, M Shapaan, J M F Ferreira *J. Thermal Anal. Calorm.* **98** 347 (2009)
[7] P Sharma, N Sharma, S Sharda, S C Katyal, V Sharma *Prog. Solid State Chem.* **44** (4) 131–141 (2016)
[8] E Akat, G Aktaş *Philos. Magazine B* **81** 689 (2001)
[9] Y Sawan, F Wakim, M El-Gabaly, M El-Rayess *J. Non-Crystal. Solids* **41** 319 (1980)
[10] C Corredor, I Quiroga, J Vazquez, J Galdon, P Villares, R Jimenez-Garay *Mater. Lett.* **42** 229 (2000)
[11] A Moharram, A Othman, H H Amer, A Dahshan *J. Non-crystal. Solids* **352** 2187 (2006)
[12] J Vázquez, C Wagner, P Villares, R Jiménez-Garay *J. Non-crystal. Solids* **235** 548 (1998)
[13] P Lopez-Alemany, J Vazquez, P Villares, R Jimenez-Garay *Thermochim. Acta* **374** 73 (2001)
[14] S H Wemple, M DiDomenico *Phys. Rev. B* **3** 1338 (1971)
[15] J Manifacier, J Gasiot, J Fillard *J. Phys. E Sci. Instrum.* **9** 1002 (1976)
[16] M El-Hagary, M Emam-Ismail, E Shaaban, A Al-Rashidi, S Althoyaib *Mater. Chem. Phys.* **132** 581 (2012)
[17] R Swanepoel *J. Phys. E Sci. Instrum.* **16** 1214 (1983)
[18] R Swanepoel *J. Phys. E Sci. Instrum.* **17** 896 (1984)
[19] E R Shaaban, G Abbady, E S Yousef, G A M Ali, S A Mahmoud, N Afify *Optoelectron. Adv. Mater. Rapid Commun.* **13** 235 (2019)
[20] E Shaaban *Mater. Chem. Phys.* **100** 411 (2006)
[21] R Vahalová, L Tichý, M Vlček, H Tichá *Phys. Status Solidi (A)* **181** 199 (2000)
[22] E R Shaaban et al. *Optik* **164** 527 (2018)
[23] C Chen et al. *Appl. Phys. Lett.* **107** 043905 (2015)
[24] G A M Ali, O A Fouad, S A Makhlouf *J. Alloys Compounds* **579** 606 (2013)
[25] F Urbach *Phys. Rev.* **92** 1324 (1953)
[26] E R Shaaban, M Y Hassaan, M Moustafa, A Qasem, G A M Ali *Optik* **186** 275 (2019)
[27] T S Moss *Butterworth, London* (1959).
[28] D Gosain, T Shimizu, M Ohmura, M Suzuki, T Bando, S Okano *J. Mater. Sci.* **26** 3271(1991)
[29] E R Shaaban, M El-Hagary, E S Moustafa, H S Hassan, Y A M Ismail, M Emam-Ismail, A S Ali *Appl. Phys. A* **122** 20 (2015)
[30] D. C. Sati, S. C. Katyal, P. Sharma *IEEE Trans. Electron. Dev.* **63**(2) 698–703 (2016)
[31] S Wemple *Phys. Rev. B* **7** 3767 (1973)
[32] M M Malik, M Zulfequar, A Kumar, M Husain *J. Phys. Condensed Matter* **4** 8331(1992)
[33] P Sharma, S Katyal *J. Appl. Phys.* **107** 113527 (2010)
[34] H Ticha, L Tichy *J. Optoelectron. Adv. Mater.* **4** 381 (2002)
[35] C C Wang *Phys. Rev. B* **2** 2045 (1970)
[36] E R Shaaban et al. *J. Am. Ceramic Soc.* **102** 4067 (2019)

Publisher's Note Springer Nature remains neutral with regard to jurisdictional claims in published maps and institutional affiliations.